Quantifying life-history trade-offs in diameter growth for tropical tree species from a large urban inventory dataset

Abstract

Trees are important ecosystem service providers that improve the physical environment and human experience in cities throughout the world. Since the ecosystem services and maintenance requirements of urban trees change as they grow in time, predictive models of tree growth rates are useful to forecast societal benefits and maintenance costs over a tree's lifetime. However, many models to date are phenomenological models with good prediction accuracies but lacking biologically interpretable parameters. This has limited our understanding of species life-history strategies for guiding tree species selection for urban plantings. In this study, we fit a diameter growth model to a large municipal tree inventory in Singapore using Bayesian inference and ordinary differential equation solver to obtain both biologically interpretable parameters and transferable predictions. We show that the 126 tree species studied here have growth parameters described by a tradeoff between fast juvenile growth when small versus slower but sustained adult growth when large, corresponding to the well-established "fast–slow" plant economics spectrum. These biological insights generally transferred well across time within the same locality; the transferability across space to a distant dataset in the United States was more variable, but it demonstrates that a biologically informed model produces more realistic predictions compared to phenomenological curve-fitting. Our findings highlight a more tangible way of selecting species for planting based not only on predicted growth, but also intuitive life-history growth characteristics that could be further generalised by functional traits to explore new species suitable for urban forestry.

Keywords

Life-history strategy; tree demography; vital rate; ontogeny; ordinary differential equation; Singapore; validation

Abbreviations

None.

Introduction

Trees play an integral role in improving the physical environment and human experience in cities (Gillerot et al., 2022; Pataki et al., 2011; Shanahan et al., 2017). In general, trees growing in urban areas require active arboricultural management to balance their social benefits (e.g., aesthetic values, heat mitigation, nature-based recreation) with potential costs (e.g., infrastructure damage, constraints on development). Urban tree management is a multi-faceted endeavour that

involves both upstream planning and integration with other urban infrastructure, and downstream site management for tree growth, removal and replacement. A key aspect of this process is the choice of tree species, which is usually based on the experience and familiarity of individual arborists with the species choices available in a given locality. The availability of municipal tree inventory datasets has made it possible to model various aspects of urban tree demography more systematically (Nowak et al., 2004; Semenzato et al., 2011), which can then objectively inform adaptive management approaches for urban forestry renewal.

Tree growth rates are a key demographic parameter for urban forests, since the ecosystem services and maintenance requirements of urban forests change as trees grow over time (Moore, 2022; Rötzer et al., 2021). For example, canopy area largely controls rainfall interception by trees and influences the amount of stormwater runoff avoided in urban areas (Dowtin et al., 2023), and the size-dependent scaling of canopy area from diameter similarly governs many other ecosystem services, such as particulate matter deposition and shading. A predictive model of tree growth rates will therefore help us to forecast provisional returns and maintenance costs over a tree's lifetime. However, many urban tree-growth studies to-date prioritise predictive accuracy of size by selecting the best out of several competing phenomenological models that are computationally less demanding, even though they lack biologically interpretable parameters (e.g., Escobedo et al., 2011; McPherson et al., 2016). In fact, the original model (McPherson and Simpson, 1999) that evolved into one of the most widely used urban forestry assessment tools, i-Tree, was initially more mechanistic (identical to the Chapman–Richards equation in Zeide 1993) but has later become more phenomenological in pursuit of prediction accuracy (McPherson et al., 2016). As such, the most popular urban forestry models to-date risk overfitting a particular dataset (Berland 2020; Thomas et al., 2019) and provide limited biological insights into how *future* urban plantings could be structured by a more general understanding of tree species' life histories.

On the other hand, parameter-heavy mechanistic models prioritise a good bottom-up understanding of size growth from cellular processes, such as photosynthesis and transpiration, which are then integrated into organismal growth (e.g., Falster et al., 2011; Moorcroft et al., 2001). As trees grow, their size (e.g., diameter) often increases in a sigmoidal manner over long time periods, reflecting a tree's propensity for exponential growth that is progressively opposed by various aging constraints (Falster et al., 2018; Zeide, 1993). The sigmoidal trajectory of diameter over a tree's lifetime translates to a rate of change (i.e., diameter growth rate) that is hump-shaped: accelerating when small but later decelerating (black line in Fig. 1). The novel contribution of our study is to capture these biological processes across a large number of species in a continuous-time growth model that represents a middle ground between phenomenological curve-fitting and mechanistic complexity. By inferring species-specific growth parameters that reflect the comparative ecology of species ontogeny, our model provides a quantitative evidence base for future species selection, especially in tropical regions with high demographic diversity (Bialic-Murphy et al., 2024) but remain data poor (Song et al., 2017).

In this study, we used a large municipal inventory in Singapore to fit a size-dependent diameter growth model to repeated measurements of trunk diameter from 176,961 trees monitored during 2010–2019. We focused on tree diameter as it is the most available measurement across urban tree inventories worldwide (Ma et al., 2021) and provides the basis for allometric scaling to other morphometric features, such as height and crown size (Feldpausch et al., 2011; Peper et al., 2014; Song et al., 2020). Using a class of model with biologically interpretable parameters to

quantify the growth characteristics of 126 tropical tree species, we show that they could facilitate species selection by ordinating species along a life-history spectrum defined by a tradeoff between juvenile and adult growth rates. We further demonstrate that these biological insights are generally transferable across time and space by validating our model's predictions (i) to a testing dataset within the same 2010–2019 period, (ii) across time to a future dataset in 2023 (same locality), and (iii) across space to an independent dataset in the United States. Furthermore, we leverage the few cases with less accurate extrapolation to discuss whether such a predictive cost is justified by the gain in generality and biological understanding in the spirit of Houlahan et al. (2016).

Material and methods

Tree inventory data

We analysed a municipal tree inventory dataset managed by the National Parks Board of Singapore (NParks), which contained measurements of trunk girth of 186,858 trees growing in public landscapes (i.e., parks and roadsides) throughout Singapore from a 9.5-year period between 1 January 2010 and 1 June 2019. Later between 1 January and 30 June 2023, a subset of the trees were remeasured and we used this as an additional dataset to validate model predictions (see *Statistical inference* below for more detail). During each inspection, trunk girth was measured 1 m above ground by a professional arborist using a flexible metal measuring tape and rounded to the nearest centimeter. Trunk girth values (m) were converted to the diameter (cm) of the circular equivalent of the measured trunk shape prior to modelling; diameter therefore had a measurement precision of ≈ 0.32 cm. Although the dataset contained tree height information in addition to tree girth, the height measurements were not used because the values were visually estimated using an ordinal scale.

From the whole dataset, we imposed a few selection criteria to remove data entries that were likely erroneous. Namely, we selected surviving trees at the time of data extraction (1 June 2019) and removed trees with girth < 0.1-m girth or very large diameters > 300 cm. As our model used species-specific parameters, we also excluded species with fewer than 100 individuals or modest variation in trunk diameter (range < 5 cm). We also removed species with fewer than 100 unique combinations of initial diameter, final diameter and time lapsed, because these species had many identical rows of records that were very likely to be entry errors. Lastly, we omitted inventory observations from members of the palm family (Arecaceae) due to the lack of secondary growth, and the hemiephiphytic strangler fig, *Ficus benjamina*, due to measurement challenges associated with its numerous, lignified column roots. The final dataset contained 176,961 trees from 126 species. For each individual tree, we limited the data to the initial and final diameter measurements (i.e., two measurements per tree) to avoid autocorrelation within each tree. Although autocorrelation due to repeated measurements within each tree can be accounted by random tree effects, in our pilot analyses we found it extremely difficult to reach model convergence because numerous trees were remeasured only once (i.e., the estimation of random effects for these trees rely on single repeated inspections). Across all trees, the time interval between first and final inspections varied from one day to 9.3 years.

Diameter growth model

Many models have been developed for organismal growth, each with their own strengths and drawbacks (e.g., Hérault et al., 2011; Paine et al., 2012; Thomas et al., 2019; Tjørve and Tjørve, 2010). For this study, we sought a middle ground between mechanistic complexity and phenomenological representation of tree diameter growth, and followed the approach adopted by Zeide (1993). Zeide reviewed a number of popular phenomenological models of tree growth (including the original model that evolved into the i-Tree program; McPherson and Simpson, 1999), starting only from those with biologically interpretable parameters, and then distilled them into a few generalised forms. All of Zeide's general model forms can be decomposed into two components: growth expansion and growth decline. In this study, we modelled the instantaneous growth rate of diameter, D, in cm per year using an equation (Zeide's "YD form", hereafter denoted as the function z) that depends only on tree size, but not tree age, since the latter is generally much harder to obtain, especially from tropical trees that lack growth rings:

$$\frac{dD}{dt} = z(D,\ a,\ b,\ c) = aD^b \exp[-c(D-1)]. \qquad (1)$$

Equation (1) includes three biologically motivated, positive-bound parameters: a, b and c. The parameter a is the growth rate at 1-cm diameter (grey dashed lines in Fig. 1), which becomes apparent when $D = 1$ is substituted into Equation (1). Zeide had originally wrote the last term as $\exp(-cD)$, but we reparameterised it slightly to $\exp[-c(D-1)]$ to let Equation (1) reduce to a when $D = 1$. Doing so changes the meaning of a from the more abstract "scaling factor" to the more tangible "growth rate at 1-cm diameter". Conveniently, 1 cm is also the lower size threshold of diameter measurement in some forest inventories.

The two components, D^b and $\exp[-c(D-1)]$, are size-dependent autoregulatory terms that represent growth expansion and growth decline, respectively. The growth expansion term D^b (blue curve in Fig. 1) reflects the innate tendency of living bodies to grow and cells to multiply (Zeide, 2003). The diameter's exponent b encapsulates the scaling up of productive organs for the uptake of photosynthates, water, and nutrients from a given diameter. In contrast, the parameter c in the growth decline term $\exp[-c(D-1)]$ (red curve in Fig. 1) captures the exponentially diminishing return of sustaining large diameters due to respiratory and overhead costs of cell maintenance, turnover and reproduction. Over a tree's lifespan, biomass build-up causes the growth decline term to eventually dominate growth expansion, thus leading to a hump-shaped growth–diameter relationship (black curve in Fig. 1), and this hump-shaped relationship leads to the sigmoidal diameter-over-time trajectories commonly observed in both the field (Camac et al., 2018; Hérault et al., 2011; Kohyama et al., 2015) and theoretical models (Falster et al., 2018).

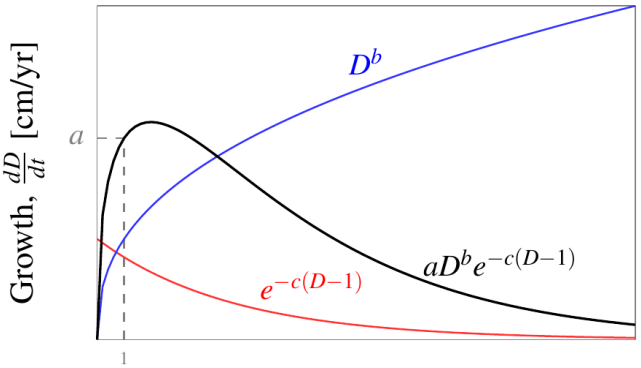

Figure 1: Conceptual diagram of a hypothetical tree species' diameter growth curve (black) given by Equation (1), which partitions the growth process into the product of two size-dependent components: growth expansion (blue) and growth decline (red).

Statistical inference

We considered several potential approaches to fit the Zeide growth model to our data. The most direct approach would be to approximate the instantaneous diameter growth rate dD/dt using discrete-time measurements by calculating $[D(t\_1) - D(t\_0)]/(t\_1 - t\_0)$, and then regress these calculated values against the initial diameter $D(t_0)$ (e.g., Hérault et al., 2011; Lai et al., 2022). However, there would be at least two shortcomings to such an approach. First, this approximation approach would be biased when diameters do not grow linearly over time, and in such cases the bias is particularly strong when a long time has lapsed between diameter measurements (see Fig. 2 for an illustrated example). Such an estimation bias would increase prediction error in tree sizes and size-dependent ecosystem functions. The second disadvantage of modelling discrete-time growth is related to the observation model–process model concept of Bayesian inference (Kuhnert, 2014): what we measure and observe in the field is girth or diameter, not growth. Growth is therefore a latent, unmeasurable process that ideally should be statistically *inferred* rather than calculated. In other words, the most appropriate response variable (outcome) of a regression is diameter, whereas growth is a process whose properties and parameters need to be inferred.

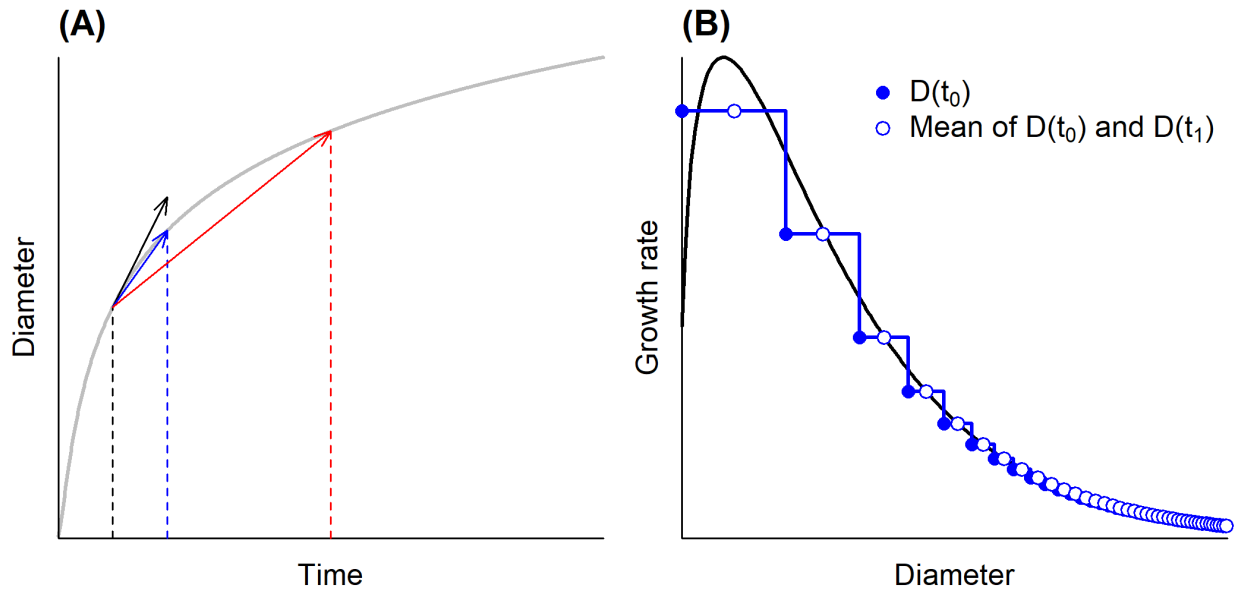

Figure 2: **(A)** Conceptual figure of potential bias in the approximation of instantaneous growth from discrete-time measurements. For a hypothetical diameter growth trajectory over time (grey curve), size-dependent diameter growth $\frac{dD}{dt}$ is the instantaneous slope at a particular diameter (black arrow, which translates to the black curve in panel **B**). Most studies, however, approximate the instantaneous growth by calculating the increment in diameter after some time interval. While such an approximation is slightly biased for short time intervals (blue), the bias becomes larger with increasing time intervals (red). In this example, discrete-time approximation of growth from a long census interval results in a considerable underestimation (red slope is much gentler than the black instantaneous slope). **(B)** Discrete approximation of instantaneous growth rate assumes a constant growth rate between census intervals (blue step-like lines), instead of a growth curve that is always adjusting to the changing diameter (black curve). When plotted or regressing against initial diameter $D(t_0)$ (a common practice in the literature), biased approximation of diameter growth from discrete measurements leads to overestimation of the instantaneous growth rate early on (blue filled circle higher than the black curve), followed quickly by underestimation later during a tree's lifespan (blue filled circle lower than the black curve). It is noteworthy that such biases can be reduced simply by plotting or regressing discrete diameter growth rates against the mean or midpoint of $D(t_0)$ and $D(t_1)$ (blue open circles), though it still is not the best approach.

To avoid these shortcomings, we leveraged the continuous-time diameter growth model given by Equation (1) to infer instantaneous diameter growth rates by solving the corresponding ordinary differential equation. Specifically, we modelled the final diameter $D_{ij}(t_1)$ of tree i in species j at time t_1 as function of its initial diameter $D_{ij}(t_0)$, elapsed time $t_1 - t_0$, and the three growth parameters a, b and c in Equation (1) in a lognormal generalised linear model (GLM):

$$D_{ij}(t_1) \sim \text{Lognormal}\left(\log\mu_{ij},\ \sigma_j\right),$$

where $\log\mu_{ij}$ and σ_j are the linear predictor and residual variance of final diameters in the lognormal GLM, respectively. The predicted final diameters μ_{ij} are estimated by finding solutions to the equation

$$\int_{D_{ij}(t_0)}^{\mu_{ij}} \frac{1}{z\left(D_{ij},\ a_j,\ b_j,\ c_j\right)} dx = t_1 - t_0\,, \qquad (2)$$

where the growth function z in the integral takes the nonlinear form described in Equation (1), except each growth parameter was allowed here to vary by species to account for interspecific variation: $z\left(D_{ij},\ a_j,\ b_j,\ c_j\right) = a_j D_{ij}^{b_j} \exp\left[-c_j\left(D_{ij} - 1\right)\right]$. The species-specific parameters (a_j, b_j and c_j) were estimated as fixed effects, i.e., without assumed correlations as in random effects. We did this to examine if any correlation between parameters would arise without prior assumption, thus providing us more confidence in concluding any tradeoff in growth strategies across species. As further elaborated in Appendix A, there is no closed-form solution for μ_{ij} in Equation (2) (i.e., the GLM predictor cannot be conventionally written with just μ_{ij} on the left-hand side). We therefore used the built-in ODE solver ode_rk45 in Stan to numerically compute μ_{ij}.

Prior to model fitting, we split 75% of the dataset into a training set (hereafter "in-sample data") to estimate parameters, and 25% into a testing set (hereafter "out-of-sample data") to validate predictions. Data splitting was performed hierarchically by species, such that each species retained 75% of its full data. The model was fitted with Bayesian inference in Stan (Stan Development Team, 2023) using the brms package v2.19.0 (Bürkner, 2021) in R v4.2.1 (R Core Team, 2022). The custom Stan code for the ODE is available on our GitHub repository. Bayesian inference was performed with 1,000 warmup and 1,000 post-warmup Hamiltonian Monte Carlo (HMC) iterations over four chains, resulting in a total of 4,000 posterior samples. We determined informative priors for the growth parameters using prior predictive checks that produced sensible predictions: $\log a_j \sim \mathrm{N}(0, 0.5)$; $\log b_j \sim \mathrm{N}(-1, 0.5)$; $\log c_j \sim \mathrm{N}(-1, 0.5)$. We increased the target average acceptance probability to 0.99 to promote chain convergence.

Biological interpretation

In addition to estimating the species-specific growth parameters a_j, b_j and c_j, we aimed to increase the utility of the model by extracting two extra pieces of information. First, we calculated the Spearman's rank correlation between the three growth parameters across the full posterior distributions as a measure of life-history tradeoff in growth strategies. For example, a strong positive correlation between two parameters indicates that species are evolutionarily or ecologically constrained to be either high or low in both growth characteristics. On the other hand, a strong negative correlation indicates that species are constrained to have high values in a growth characteristic but have low values in another. We chose the nonparametric rank correlation to preserve the correlation between growth parameters in both arithmetic and logarithmic scales (skewed distributions are expected for the positive-bound parameters).

Model assessments

We assessed the transferability of our model's biological insights across time and space. First, we compared the residuals (difference between observed and predicted final diameters) of the in-sample data to that of the out-of-sample data to examine prediction accuracy. Second, to examine the temporal transferability of our model's prediction, we validated the short-term forecasts on a subset of 23,621 trees and species that were remeasured in 2023 (four years since the last measurement in the core dataset). The 2023 predictions were made from the last measured diameter of each tree in the 2010–2019 data. That is, every tree differs in the amount of time lapsed, which ranged from 3.7 to 11.9 years. Similarly, we examined R^2 and model residuals to assess the goodness-of-fit of the temporal extrapolation.

Additionally, we examined the spatial transferability of our model by validating predictions on one of the most widely referenced urban tree datasets in the United States (McPherson et al., 2016). Initially, we attempted to validate our model against other datasets within the same biogeographical region but were not able to do so due to the extreme scarcity of open data in the Tropics. The US dataset shared ten of our species, measured from 453 trees in Hawaii and the southern Californian coast. To assess how well our model extrapolated to the US dataset, we calculated the log-likelihood ratio of our out-of-sample posterior predictions to the log-likelihood of McPherson's in-sample point predictions. A log-likelihood ratio of 1 indicates that our out-of-sample predictions have identical fit as McPherson's in-sample predictions, whereas a log-likelihood ratio of > 1 indicates that the US data are more likely to be reproduced by our out-of-sample predictions compared to McPherson's in-sample prediction, and vice versa.

Results

The 126 tree species varied greatly in growth characteristics, as reflected by the three species-specific parameters a, b and c (Fig. S1 and Table S1). The growth parameters spanned three orders of magnitude, with diameter growth rate at 1 cm (a) having the greatest range (0.5–12.6 cm/yr), followed by the growth expansion factor (b, range = 0.06–4.61) and lastly the growth decline factor (c, range = 0.03–1.30). These growth characteristics were not fully independent; the parameter a was moderately correlated with b (Spearman's $r = -0.31$; Fig. S1A), whereas a and c were very weakly correlated ($r = 0.09$; Fig. S1B). In contrast, the strongest correlation was the positive relationship between b and c ($r = 0.49$; Fig. S1C).

In the following sections, we focus the on the positive correlation between the growth expansion factor b and the growth decline factor c, which are the two size-dependent parameters that provide the deepest insights into the life-history tradeoffs among species (Fig. 3). Most species were either high in both b and c, or low in both parameters. Few to none of the species were found in other regions of the b–c parameter space. The high b–high c species displayed more sigmoidal diameter trajectories over time in Fig. 4A or a more peaked growth–diameter relationship in Fig. 4B, leading to much faster growth rates when small that then decelerate rapidly. In contrast, the low b–low c species' diameter trajectories over time and growth–diameter relationships were less curved, leading to slower growth rates when small but sustaining growth rates longer into larger sizes.

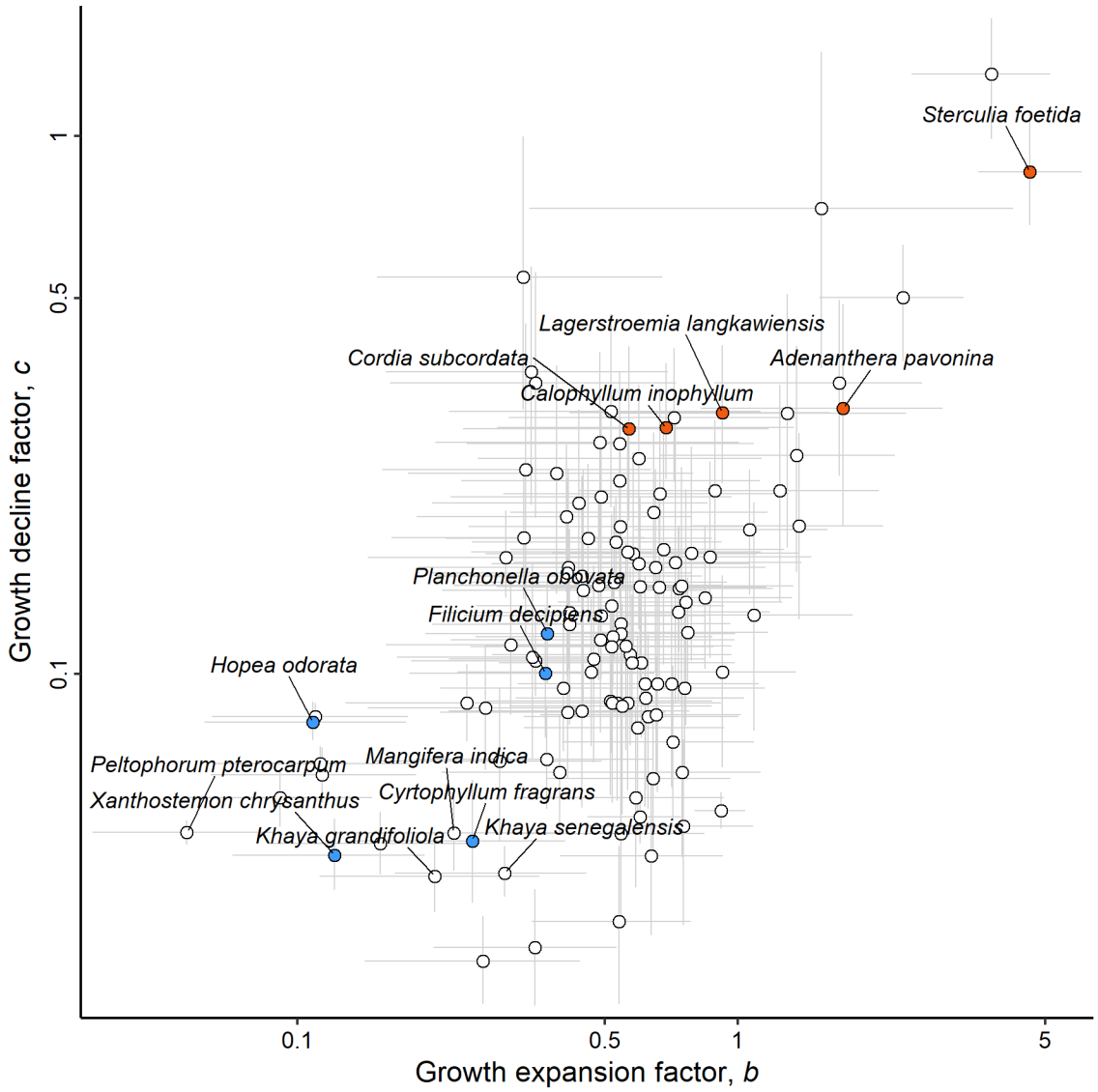

Figure 3: Life-history tradeoff in diameter growth as inferred from the correlation between the growth expansion factor, b, and the growth decline factor, c. Points and error bars are median and 89% credible intervals (CIs), respectively, of the posterior. The labelled points are example species used in the *Discussion*: red = high b–high c species; blue = low b–low c species; white with label = species estimates with caveats. Note the log-scale on both axes.

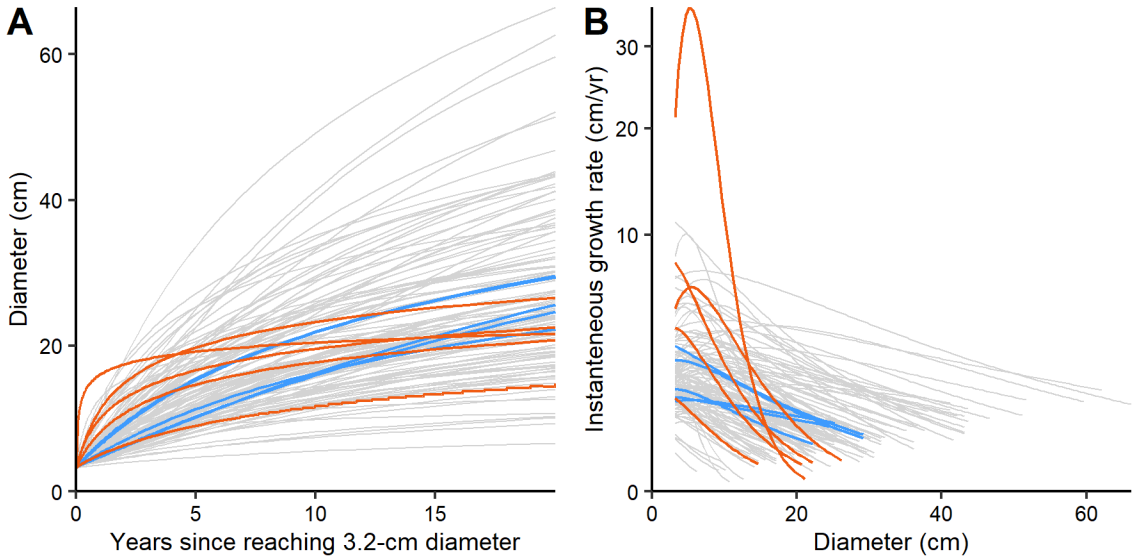

Figure 4: **(A)** Expected diameter trajectories of species from an initial diameter of 3.2 cm (≈ 10 cm girth, which is a common size at planting in our study area) over 20 years. **(B)** The instantaneous growth rates (instantaneous slopes of each trajectory in **A**) in relation to diameter. Each line denotes the median posterior prediction of a species. Coloured lines are the same set of example species in Fig. 3: red = high b–high c species; blue = low b–low c species. Note the square-root scale of the Y-axis in **B**.

In terms of goodness-of-fit, our model had $R^2 = 0.88$ for both the 2010–2019 in-sample and out-of-sample final tree diameters. In-sample and out-of-sample prediction accuracies were fairly high, both with a median residual of 0.3 cm (Figs S2 and S3). The residual ranges of both in- and out-of-sample predictions were also very similar: 50% of residuals fell between -2.6 and 4.1 cm, while 89% fell between -8.9 and 13.5 cm. We consider these residuals to be reasonable given that a median-sized tree in our dataset was 33.4 cm, with an interquartile range of 19.1–50.9 cm. Increasing the time lapsed between initial and final diameter measurements did not seem to reduce prediction accuracy, as the median residuals stayed close to zero, even if the range of residuals increased slightly (Fig. S2).

The temporal transferability of predictions to the 2023 data also extrapolated well, with $R^2 = 0.93$ and 96% of observations within the prediction intervals; the median residual was -0.2 cm, with 89% of residuals falling between -8.7 and 10.8 cm (Figs S2 and S3). The spatial transferability of predictions to the US dataset (McPherson et al., 2016) also extrapolated well considering the 10,000-km distance between datasets (Fig. 5). Half of the ten shared species had log-likelihoods of ≥ 1, indicating that our out-of-sample predictions on them were comparable or better than the in-sample predictions of McPherson et al. (2016). For the other half, their log-likelihoods was < 1 but not severely low (except for one species, *Melaleuca citrina*), and many of their data points still fell within our prediction intervals.

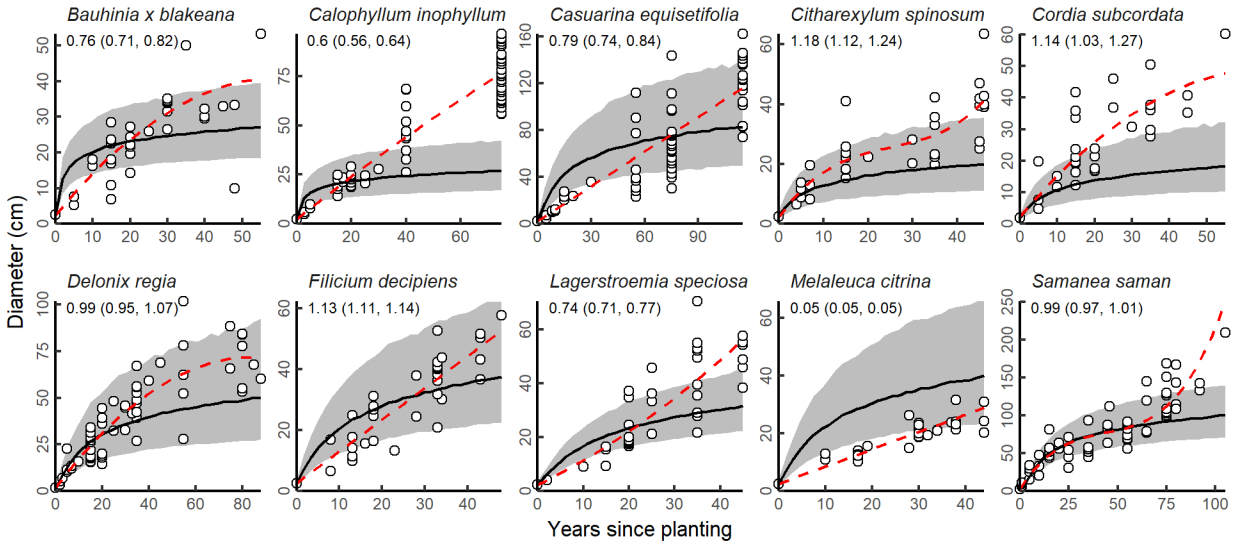

Figure 5: Spatial transferability of our model (trained on a dataset in Singapore) to the growth trajectories of ten shared species in a US dataset. Open circles and red dashed lines are US data and in-sample fit from McPherson et al. (2016), whereas black lines and shaded areas are posterior median and 89% CIs of our out-of-sample predictions. Values on the top-left corner of each panel show the log-likelihood ratio between ours and McPherson et al.'s (2016) models, respectively (89% CIs in parentheses).

Discussion

In this study, we quantified the growth characteristics of 126 tropical tree species using an urban tree inventory dataset comparable to some of the largest existing forest inventories (e.g., Anderson-Teixeira et al., 2015; Vidal et al., 2016). Distinct from similar work in temperate climates (Schelhaas et al., 2018), it was possible to model diameter growth for many more species due to the high demographic diversity supported by our study site's tropical environment (Bialic-Murphy et al., 2024), which facilitates a more comprehensive comparison of life-history strategies across species. We demonstrated that growth models can serve beyond their predictive purpose; they can also include biologically-interpretable parameters that characterise tree growth strategies along the "fast–slow" plant economics spectrum (Reich, 2014) (i.e., tree species tend to either grow faster when small and then decelerate rapidly or grow slower when small but sustain growth over a longer lifespan).

Life-history tradeoff in diameter growth

Reich (2014) posited a unified "fast–slow" plant economics spectrum, along which a trade-off exists between traits optimising growth rates under high resource availability conditions and traits optimising survival under low resource availability conditions. Our findings reinforce this theory with the correlation between the growth expansion factor b and the growth decline factor c (Fig. 3). The 126 tree species seemed to be constrained to either be high in both b and c

(growing fast when small), or low in both (growing slow when small but sustained growth when large). Practically no species were found in the high *b*–low *c* quadrant (fast growth throughout all size classes). The high *b*–high *c* species (e.g., *Adenanthera pavonina*, *Calophyllum inophyllum*, *Cordia subcordata*, *Lagerstroemia langkawiensis* and *Sterculia foetida*) that grow faster when small eventually grow slower than the low *b*–low *c* species (e.g., *Cyrtophyllum fragrans*, *Filicium decipiens*, *Hopea odorata*, *Planchonella obovata*, *Xanthostemon chrysanthus*; Fig. 3B). Thus, species that exhibit rapid growth during early life stages tend not to sustain this growth in subsequent growth phases. These life-history tradeoffs likely reflect several underlying processes, such as trees that grow fast and die fast reaching their natural mature size earlier for reproduction (Wenk and Falster, 2015), a trade-off between fast growth and tree hydraulic and mechanical safety (Eller et al., 2018), and a trade-off between intrinsic cell metabolism and deterioration in cell function (Brienen et al., 2020).

Moreover, our results imply a nuanced interpretation of "fast growth": species at opposite ends of the life-history spectrum (high *b*–high *c* versus low *b*–low *c*) display contrasting instantaneous diameter growth curves that cross one another over time, resulting in an ontogenetic rank swap in growth rates (Fig. 4B). Both species groups grow faster than one another, but at different sizes or life stages. Such an ontogenetic rank swap in growth rates may also reconcile some species parameters that we initially thought were counterintuitive; a few species that are known to grow fast had low growth expansion factor *b* (e.g., *Khaya* spp., *Mangifera indica* and *Peltophorum pterocarpum*), but perhaps their fast-growing characteristics are better captured by the also-low growth decline factor *c* (Fig. 3). This also reflects that our horticulture knowledge of these species mainly came from more mature and established individuals, which also aligns with the fact that these species mostly consisted of larger trees on the ground.

To further strengthen our mechanistic understanding, future work could identify plant functional traits that underpin such a life-history tradeoff. "Soft" functional traits that are more easily available, such as wood density and specific leaf area, are promising predictors of the growth parameters (Hérault et al., 2011; Thomas et al., 2019), whereas "hard" physiological traits that are more labour intensive to measure, such as xylem hydraulic conductivity and photosynthetic rate, provide even finer insights into how cellular functions scale to organismal growth (Falster et al., 2011; He et al., 2022; Reich, 2014). These traits can be used, for example, to test if tree species are evolutionarily restricted from having high growth expansion and low growth decline factors to always grow fast (i.e., the dearth of species in the bottom-right quadrant of Fig. 3). We showed that species with fast growth when small also have slower growth when they are large, thus attaining lower maximum sizes. Such a tradeoff could be related to hydraulic traits that permit highly energetic growth when small, but set an upper limit on tree stature due to difficulties in transporting water to the canopy (Liu et al., 2019; Poorter et al., 2010).

Practical applications for species selection

Our growth model offers the direct use of growth parameters to select species with the preferred life-history characteristics for specific landscape contexts. For example, species that grow rapidly up to a relatively small mature size (high *b*–high *c*) would be suitable candidates for urban sites where it is desirable to have high foliage cover from the outset (e.g., park entrances). On the other end of the life-history spectrum, species that grow more slowly when small but

show slower decline in growth rates when large (low b–low c) would be more appropriate for urban locations where the land use is expected to be more stable (e.g., heritage areas). Certain species at the peripheries of the overall growth-rate tradeoff may warrant particular attention in terms of planting strategy. For example, species showing fairly high growth rates across all size classes (low c but relatively high b) are not likely to be suitable for constrained urban spaces, given their propensity for long-term growth (e.g., *Alstonia angustifolia*, *Cinnamomum iners*, *Delonix regia* and *Samanea saman*). More generally for urban forest management, the diameter growth rates obtained from the model would be useful to optimise planting strategy in particular sites, for example, by combining both fast-growing and slower-growing tree species to achieve shade provision over the shorter term, while sustaining the longer-term needs for shade and other environmental benefits through the slower-growing species that requires less maintenance. Nevertheless, it should be acknowledged that there are other relevant factors to consider for urban trees besides growth rates, such as structural safety, habitat value for wildlife, aesthetics, native conservation status, and susceptibility to disease (Conway and Vander Vecht, 2015; Trowbridge and Bassuk, 2004).

Transferability of biological insights

To assess how transferable these tree growth characteristics are across space and time, we validated our model's predictions with data from the same locality within the same period (2010–2019) and in the future (2023), as well as an independent dataset in the United States (McPherson et al., 2016). When transferring to the same period or future within the same locality, our model compared favourably in terms of prediction accuracy to existing empirical models of urban tree growth, which have reported elsewhere R^2 values around 0.5–0.9 (e.g., McPherson et al., 2016; Semenzato et al., 2011). Prediction accuracy as log-likelihood ratio also performed well for five out of ten species when our model was transferred to a different locality in the US, and was only severely low for one species. For some of the species with poorer spatial transferabilities, such as *Calophyllum inophyllum*, it is crucial to note that its extrapolation held up to 30–40 years since planting when many ecological forecasts only remain accurate within days to weeks (Lewis et al., 2022). Furthermore, many of the previous growth models with high goodness-of-fit are polynomial equations intended only for a certain number of years since planting but extrapolate spuriously into the future (Paine et al., 2012). For example, the fitted polynomial for *Samanea saman* would project a doubling in diameter to ~400 cm at 120 years since planting, whereas our model would predict ~70–150 cm guided by the biological understanding that growth decelerates in larger trees due to resource reallocation to reproduction and biomass turnover (Falster et al., 2018). It is also noteworthy that although our model underestimated the diameter growth of *Cordia subcordata* in the US data, our model still had a better fit than McPherson et al.'s (2016) in-sample fit as judged by log-likelihood; this was because the species was reported to have very large residual variance in the original analysis, which was prone to predicting negative diameters. We were unable to check if the reported variance was an entry error because we were unable to reproduce the original model fit.

Nonetheless, it is important to address real-world factors that challenge extrapolation. Similar to Shoda et al. (2020), we also found that the species in our dataset tended to grow slower than their US counterparts, resulting in smaller diameters and thus underestimations in the long run. These underestimations could be due to missing exogenous factors in our model, such as abiotic environment (e.g., climate and soil properties) and management practices (e.g., pruning and

fertilization), which would have contributed to error in prediction or parameter estimations (Rötzer et al., 2021). It is possible that the same species in our study area experienced tighter growing space than their US counterparts. Competitive pressure from neighbouring trees may also become an increasingly important driver of urban tree growth (Brienen and Zuidema, 2006; Schelhaas et al., 2018), and many studies have examined suitable size-dependent growth models accounting for the biotic interactions among forest trees (e.g., Lai et al., 2022; Rüger et al., 2011). Additionally, the inclusion of maintenance records containing information about the cultural practices used to care for trees will be especially useful (Shoda et al., 2020). Accordingly, we recommend future tree growth models to include both traits and environments, as well as their interaction, as moderators of tree growth parameters.

Although the range of our predicted diameter growth rates overlapped with values reported for other species in natural forests (e.g., Hérault et al., 2011; Kohyama et al., 2015; Rüger et al., 2011), our trees could display growth rates up to a magnitude greater similar to the urban trees in McPherson et al. (2016). For example, a *Swietenia macrophylla* tree with a diameter of 10–20 cm was reported to grow at about 0.5 cm yr^{-1} in its native Amazonian range (Grogan et al., 2014), but the same-sized trees in our study location grew over 2.0 cm yr^{-1} on average. The main reason for the higher growth rates in our study was likely because the trees in our dataset typically grew under high-light, open conditions compared to their natural or managed forest habitats (Smith et al., 2019). Moreover, many species in our dataset originated from tropical monsoon climates with pronounced dry seasons, whereas our study location lacks an extensive dry season and would therefore be more conducive to the year-round growth of these species compared to their habitat of origin. Furthermore, unusually early peak growth rates could reflect the arboricultural practice of providing compost and supplementary irrigation during the establishment stage.

Limitations and future directions

We have quantified the growth characteristics of 126 species with sufficient data, yet there remain more than a thousand tree species in Singapore with incomplete ontogeny (National Parks Board, 2024). Practitioners may wish to consider new candidate species under different circumstances, for example to design a planting palette that includes more under-studied native species or one that is more tolerant to future climate change (Laughlin et al., 2018). For these applications, a good understanding of trait–demography relationships will allow us to extrapolate predictions onto new species (e.g., Hérault et al., 2011). This research direction is a promising avenue given the increased accessibility of global and regional trait databases (e.g., Falster et al., 2021; Kattge et al., 2011). Although trait-based theories of plant demography are mostly established from unmanaged forests, recent urban studies suggest that these trait–demography relationships are also generalisable to more managed settings (Simovic et al., 2024; Watkins et al., 2021).

Although diameter is the most fundamental and measurable basis of tree growth on which other dimensions are derived via allometric scaling (McPherson et al., 2016; Rötzer et al., 2021), our study did not consider the other dimensions such as height, branch length and crown area to provide a more complete evaluation of ecosystem services and maintenance over a tree's lifetime (Dowtin et al., 2023; Moore 2022). Compared to natural forests (e.g., Jucker et al., 2022), efforts to collect data and model allometry for large numbers of species comparable to our study remain low in tropical urban forestry (Rötzer et al., 2021; Roy et al., 2012; but see Song et al., 2020).

Addressing this knowledge gap will greatly realise the potential of tropical cities in leveraging their rich biodiversity to select species that provide multiple benefits and fulfil local needs (Song et al., 2017).

Conclusions

We have demonstrated that it is feasible to fit models with biologically interpretable parameters to municipal tree growth records with acceptable transferability, thus granting insights into the comparative life histories of tree species in tropical urban landscapes. By identifying the position of species along the established fast–slow continuum, our findings provide a quantitative evidence base to select species for planting based on preferred growth characteristics. We hope that this approach will empower urban tree managers to take bolder steps to respond dynamically to diverse selection pressures on urban tree performance, backed by empirical data.

Data statement

The data that has been used is confidential. Codes for the model will be archived on GitHub/Zenodo with a DOI link upon acceptance.

References

Anderson-Teixeira, K. J., Davies, S. J., Bennett, A. C., Gonzalez-Akre, E. B., Muller-Landau, H. C., Joseph Wright, S., Abu Salim, K., Almeyda Zambrano, A. M., Alonso, A., Baltzer, J. L., Basset, Y., Bourg, N. A., Broadbent, E. N., Brockelman, W. Y., Bunyavejchewin, S., Burslem, D. F. R. P., Butt, N., Cao, M., Cardenas, D., … Zimmerman, J. (2015). CTFS-ForestGEO: A worldwide network monitoring forests in an era of global change. Global Change Biology, 21(2), 528–549. https://doi.org/10.1111/gcb.12712

Berland, A. (2020). Urban tree growth models for two nearby cities show notable differences. Urban Ecosystems, 23(6), 1253–1261. https://doi.org/10.1007/s11252-020-01015-0

Bialic-Murphy, L., McElderry, R. M., Esquivel-Muelbert, A., van den Hoogen, J., Zuidema, P. A., Phillips, O. L., de Oliveira, E. A., Loayza, P. A., Alvarez-Davila, E., Alves, L. F., Maia, V. A., Vieira, S. A., Arantes da Silva, L. C., Araujo-Murakami, A., Arets, E., Astigarraga, J., Baccaro, F., Baker, T., Banki, O., … Crowther, T. W. (2024). The pace of life for forest trees. *Science*, *386*(6717), 92–98. https://doi.org/10.1126/SCIENCE.ADK9616

Brienen, R.J.W., Caldwell, L., Duchesne, L., Voelker, S., Barichivich, J., Baliva, M., Ceccantini, G., Di Filippo, A., Helama, S., Locosselli, G.M., Lopez, L., Piovesan, G., Schöngart, J., Villalba, R., Gloor, E., 2020. Forest carbon sink neutralized by pervasive growth-lifespan trade-offs. Nature Communications 11, 1–10. https://doi.org/10.1038/s41467-020-17966-z

Brienen, R.J.W., Zuidema, P.A., 2006. The use of tree rings in tropical forest management: Projecting timber yields of four Bolivian tree species. Forest Ecology and Management 226, 256–267. https://doi.org/10.1016/j.foreco.2006.01.038

Bürkner, P.-C., 2021. Bayesian item response modeling in R with brms and Stan. Journal of Statistical Software 100, 1–54. https://doi.org/10.18637/jss.v100.i05

Camac, J.S., Condit, R., FitzJohn, R.G., McCalman, L., Steinberg, D., Westoby, M., Joseph Wright, S., Falster, D.S., 2018. Partitioning mortality into growth-dependent and growth-independent hazards across 203 tropical tree species. Proceedings of the National Academy of Sciences of the United States of America 115, 12459–12464. https://doi.org/10.1073/pnas.1721040115

Conway, T.M., Vander Vecht, J., 2015. Growing a diverse urban forest: Species selection decisions by practitioners planting and supplying trees. Landscape and Urban Planning 138, 1–10. https://doi.org/10.1016/j.landurbplan.2015.01.007

Dowtin, A.L., Cregg, B.C., Nowak, D.J., Levia, D.F., 2023. Towards optimized runoff reduction by urban tree cover: A review of key physical tree traits, site conditions, and management strategies. Landscape and Urban Planning 239, 104849. https://doi.org/10.1016/j.landurbplan.2023.104849

Eller, C.B., de V. Barros, F., R.L. Bittencourt, P., Rowland, L., Mencuccini, M., S. Oliveira, R., 2018. Xylem hydraulic safety and construction costs determine tropical tree growth. Plant Cell and Environment 41, 548–562. https://doi.org/10.1111/pce.13106

Escobedo, F.J., Kroeger, T., Wagner, J.E., 2011. Urban forests and pollution mitigation: Analyzing ecosystem services and disservices. Environ. Pollut. 159, 2078–2087.

Falster, A. D., Gallagher, R., Wenk, E., Wright, I., Indiarto, D., Andrew, S. C., Lawson, J., Allen, S., Fuchs, A., Adams, M. A., Collin, W., Alfonzetti, M., Angevin, T., Atkin, O. K., Auld, T., Baker, A., Buckton, G., Burrows, G., Caldwell, E., … Kasia Ziemińska. (2021). AusTraits – a curated plant trait database for the Australian flora. Nature Scientific Data, 8(1), 254. https://doi.org/10.1038/s41597-021-01006-6

Falster, D.S., Brannstrom, A., Dieckmann, U., Westoby, M., 2011. Influence of four major plant traits on average height, leaf-area cover, net primary productivity, and biomass density in single-species forests: A theoretical investigation. Journal of Ecology 99, 148–164. https://doi.org/10.1111/j.1365-2745.2010.01735.x

Falster, D.S., Duursma, R.A., FitzJohn, R.G., 2018. How functional traits influence plant growth and shade tolerance across the life cycle. Proceedings of the National Academy of Sciences of the United States of America 115, E6789–E6798. https://doi.org/10.1073/pnas.1714044115

Feldpausch, T. R., Banin, L., Phillips, O. L., Baker, T. R., Lewis, S. L., Quesada, C. A., Affum-Baffoe, K., Arets, E. J. M. M., Berry, N. J., Bird, M., Brondizio, E. S., De Camargo, P., Chave, J., Djagbletey, G., Domingues, T. F., Drescher, M., Fearnside, P. M., França, M. B., Fyllas, N. M., … Lloyd, J. (2011). Height-diameter allometry of tropical forest trees. *Biogeosciences*, *8*(5), 1081–1106. https://doi.org/10.5194/bg-8-1081-2011

Gillerot, L., Landuyt, D., Oh, R., Chow, W., Haluza, D., Ponette, Q., Jactel, H., Bruelheide, H., Jaroszewicz, B., Scherer-Lorenzen, M., De Frenne, P., Muys, B., & Verheyen, K. (2022). Forest

structure and composition alleviate human thermal stress. *Global Change Biology*, *28*(24), 7340–7352. https://doi.org/10.1111/gcb.16419

Grogan, J., Landis, R.M., Free, C.M., Schulze, M.D., Lentini, M., Ashton, M.S., 2014. Big-leaf mahogany Swietenia macrophylla population dynamics and implications for sustainable management. Journal of Applied Ecology 51, 664–674. https://doi.org/10.1111/1365-2664.12210

He, P., Lian, J., Ye, Q., Liu, H., Zheng, Y., Yu, K., Zhu, S., Li, R., Yin, D., Ye, W., Wright, I.J., 2022. How do functional traits influence tree demographic properties in a subtropical monsoon forest? Functional Ecology 36, 3200–3210. https://doi.org/10.1111/1365-2435.14189

Hérault, B., Bachelot, B., Poorter, L., Rossi, V., Bongers, F., Chave, J., Paine, C.E.T., Wagner, F., Baraloto, C., 2011. Functional traits shape ontogenetic growth trajectories of rain forest tree species. Journal of Ecology 99, 1431–1440. https://doi.org/10.1111/j.1365-2745.2011.01883.x

Houlahan, J. E., McKinney, S. T., Anderson, T. M., & McGill, B. J. (2017). The priority of prediction in ecological understanding. *Oikos, 126*(1), 1–7. https://doi.org/10.1111/oik.03726

Jucker, T., Fischer, F. J., Chave, J., Coomes, D. A., Caspersen, J., Ali, A., Loubota Panzou, G. J., Feldpausch, T. R., Falster, D., Usoltsev, V. A., Adu-Bredu, S., Alves, L. F., Aminpour, M., Angoboy, I. B., Anten, N. P. R., Antin, C., Askari, Y., Muñoz, R., Ayyappan, N., … Zavala, M. A. (2022). Tallo: A global tree allometry and crown architecture database. Global Change Biology, 28(17), 5254–5268. https://doi.org/10.1111/gcb.16302

Kattge, J., Díaz, S., Lavorel, S., Prentice, I. C., Leadley, P., Bönisch, G., Garnier, E., Westoby, M., Reich, P. B., Wright, I. J., Cornelissen, J. H. C., Violle, C., Harrison, S. P., Van Bodegom, P. M., Reichstein, M., Enquist, B. J., Soudzilovskaia, N. A., Ackerly, D. D., Anand, M., … Wirth, C. (2011). TRY - a global database of plant traits. *Global Change Biology*, *17*(9), 2905–2935. https://doi.org/10.1111/j.1365-2486.2011.02451.x

Kohyama, T.S., Potts, M.D., Kohyama, T.I., Kassim, A.R., Ashton, P.S., 2015. Demographic Properties Shape Tree Size Distribution in a Malaysian Rain Forest. The American Naturalist 185, 367–379. https://doi.org/10.1086/679664

Kuhnert, P., 2014. Physical-statistical modelling. Environmetrics 25, 201–202. https://doi.org/10.1002/env.2276

Lai, H.R., Chong, K.Y., Yee, A.T.K., Mayfield, M.M., Stouffer, D.B., 2022. Non-additive biotic interactions improve predictions of tropical tree growth and impact community size structure. Ecology 103, e03588. https://doi.org/10.1002/ecy.3588

Laughlin, D.C., Chalmandrier, L., Joshi, C., Renton, M., Dwyer, J.M., Funk, J.L., 2018. Generating species assemblages for restoration and experimentation: A new method that can simultaneously converge on average trait values and maximize functional diversity. Methods in Ecology and Evolution 9, 1764–1771. https://doi.org/10.1111/2041-210X.13023

Lehtonen, J., 2016. The Lambert W function in ecological and evolutionary models. Methods in Ecology and Evolution 7, 1110–1118. https://doi.org/10.1111/2041-210X.12568

Lewis, A. S. L., Woelmer, W. M., Wander, H. L., Howard, D. W., Smith, J. W., McClure, R. P., Lofton, M. E., Hammond, N. W., Corrigan, R. S., Thomas, R. Q., & Carey, C. C. (2022). Increased adoption of best practices in ecological forecasting enables comparisons of forecastability. *Ecological Applications*, *32*(2), 1–16. https://doi.org/10.1002/eap.2500

Liu, H., Gleason, S.M., Hao, G., Hua, L., He, P., Goldstein, G., Ye, Q., 2019. Hydraulic traits are coordinated with maximum plant height at the global scale. Science Advances 5. https://doi.org/10.1126/sciadv.aav1332

Ma, B., Hauer, R. J., Östberg, J., Koeser, A. K., Wei, H., & Xu, C. (2021). A global basis of urban tree inventories: What comes first the inventory or the program. *Urban Forestry and Urban Greening*, *60*(November 2020). https://doi.org/10.1016/j.ufug.2021.127087

Mcpherson, E. G., & Simpson, J. R. (1999). Carbon Dioxide Reduction Through Urban Forestry: Guidelines for Professional and Volunteer Tree Planters. In *Gen. Tech. Rep. PSW- GTR-171*. Pacific Southwest Research Station, Forest Service, U.S. Department of Agriculture.

McPherson, E.G., Doorn, N. van, Peper, P.J., 2016. Urban Tree Database and Allometric Equations. General Technical Report PSW-GTR-253 86.

Moorcroft, P.R., Hurtt, G.C., Pacala, S.W., 2001. A method for scaling vegetation dynamics: The ecosystem demography model (ED). Ecological Monographs 71, 557–586. https://doi.org/10.1890/0012-9615(2001)071[0557:AMFSVD]2.0.CO;2

Moore, G.M., 2022. Lifetime cost models for large, long-lived, street trees in Australia. Arboricultural Journal 44, 21–41. https://doi.org/10.1080/03071375.2021.2014689

National Parks Board. (2024). TreesSG. https://www.nparks.gov.sg/treessg

Nowak, D.J., Kuroda, M., Crane, D.E., 2004. Tree mortality rates and tree population projections in Baltimore, Maryland, USA. Urban Forestry and Urban Greening 2, 139–147. https://doi.org/10.1078/1618-8667-00030

Paine, C.E.T., Marthews, T.R., Vogt, D.R., Purves, D., Rees, M., Hector, A., Turnbull, L.A., 2012. How to fit nonlinear plant growth models and calculate growth rates: An update for ecologists. Methods in Ecology and Evolution 3, 245–256. https://doi.org/10.1111/j.2041-210X.2011.00155.x

Pataki, D.E., Carreiro, M.M., Cherrier, J., G., N. E., J., V., Pincetl, S., Pouyat, R.V., Whitlow, T.H., Zipperer, W.C., 2011. Coupling biogeochemical cycles in urban environments: Ecosystem services, green solutions, and misconceptions. Frontiers in Ecology and the Environment 9, 27–36.

Peper, P. J., Alzate, C. P., McNeil, J. W., & Hashemi, J. (2014). Allometric equations for urban ash trees (fraxinus spp.) in oakville, southern ontario, Canada. Urban Forestry and Urban Greening, 13(1), 175–183. https://doi.org/10.1016/j.ufug.2013.07.002

Poorter, L., McDonald, I., Alarcón, A., Fichtler, E., Licona, J.C., Peña-Claros, M., Sterck, F., Villegas, Z., Sass-Klaassen, U., 2010. The importance of wood traits and hydraulic conductance

for the performance and life history strategies of 42 rainforest tree species. New Phytologist 185, 481–492. https://doi.org/10.1111/j.1469-8137.2009.03092.x

R Core Team, 2022. R: A language and environment for statistical computing. R Foundation for Statistical Computing, Vienna, Austria.

Reich, P.B., 2014. The world-wide 'fast-slow' plant economics spectrum: A traits manifesto. Journal of Ecology 102, 275–301. https://doi.org/10.1111/1365-2745.12211

Rötzer, T., Moser-Reischl, A., Rahman, M.A., Grote, R., Pauleit, S., Pretzsch, H., 2021. Modelling urban tree growth and ecosystem services: Review and perspectives, in: Cánovas, F.M., Lüttge, U., Risueño, M.-C., Pretzsch, H. (Eds.), Progress in Botany Vol. 82. Springer International Publishing, Cham, pp. 405–464. https://doi.org/10.1007/124_2020_46

Roy, S., Byrne, J., & Pickering, C. (2012). A systematic quantitative review of urban tree benefits, costs, and assessment methods across cities in different climatic zones. *Urban Forestry and Urban Greening*, *11*(4), 351–363. https://doi.org/10.1016/j.ufug.2012.06.006

Rüger, N., Berger, U., Hubbell, S.P., Vieilledent, G., Condit, R., 2011. Growth strategies of tropical tree species: Disentangling light and size effects. PLoS ONE 6, e25330. https://doi.org/10.1371/journal.pone.0025330

Schelhaas, M.J., Hengeveld, G.M., Heidema, N., Thürig, E., Rohner, B., Vacchiano, G., Vayreda, J., Redmond, J., Socha, J., Fridman, J., Tomter, S., Polley, H., Barreiro, S., Nabuurs, G.J., 2018. Species-specific, pan-European diameter increment models based on data of 2.3 million trees. Forest Ecosystems 5. https://doi.org/10.1186/s40663-018-0133-3

Semenzato, P., Cattaneo, D., Dainese, M., 2011. Growth prediction for five tree species in an Italian urban forest. Urban Forestry and Urban Greening 10, 169–176. https://doi.org/10.1016/j.ufug.2011.05.001

Shanahan, D.F., Cox, D.T.C., Fuller, R.A., Hancock, S., Lin, B.B., Anderson, K., Bush, R., Gaston, K.J., 2017. Variation in experiences of nature across gradients of tree cover in compact and sprawling cities. Landscape and Urban Planning 157, 231–238.

Shoda, T., Imanishi, J., & Shibata, S. (2020). Growth characteristics and growth equations of the diameter at breast height using tree ring measurements of street trees in Kyoto City, Japan. *Urban Forestry and Urban Greening*, *49*, 126627. https://doi.org/10.1016/j.ufug.2020.126627

Simovic, M., Mueller, K.E., McMahon, S.M., Medeiros, J.S., 2024. Functional traits and size interact to influence growth and carbon sequestration among trees in urban greenspaces. Functional Ecology 38, 967–983. https://doi.org/10.1111/1365-2435.14505

Smith, I.A., Dearborn, V.K., Hutyra, L.R., 2019. Live fast, die young: Accelerated growth, mortality, and turnover in street trees. PLoS ONE 14, e0215846.

Song, X. P., Richards, D., Edwards, P., & Tan, P. Y. (2017). Benefits of trees in tropical cities. *Science*, *356*(6344), 1241–1242. https://doi.org/10.1126/science.aan6642

Song, X.P., Lai, H.R., Wijedasa, L.S., Tan, P.Y., Edwards, P.J., Richards, D.R., 2020. Height–diameter allometry for the management of city trees in the tropics. Environmental Research Letters 15, 114017. https://doi.org/10.1088/1748-9326/abbbad

Stan Development Team, 2023. RStan: The R interface to Stan.

Thomas, F.M., Yen, J.D.L., Vesk, P.A., 2019. Using functional traits to predict species growth trajectories, and cross-validation to evaluate these models for ecological prediction. Ecology and Evolution 9, 1554–1566. https://doi.org/10.1002/ece3.4693

Tjørve, E., Tjørve, K.M.C., 2010. A unified approach to the Richards-model family for use in growth analyses: Why we need only two model forms. Journal of Theoretical Biology 267, 417–425. https://doi.org/10.1016/j.jtbi.2010.09.008

Trowbridge, P.J., Bassuk, N.L., 2004. Trees in the Urban Landscape: Site Assessment, Design, and Installation. John Wiley & Sons., New York, NY.

Vidal, C., Alberdi, I.A., Mateo, L.H., Redmond, J.J. (Eds.), 2016. National Forest Inventories: Assessment of Wood Availability and Use. Springer.

Watkins, H., Hirons, A., Sjöman, H., Cameron, R., Hitchmough, J.D., 2021. Can Trait-Based Schemes Be Used to Select Species in Urban Forestry? Frontiers in Sustainable Cities 3, 1–37. https://doi.org/10.3389/frsc.2021.654618

Wenk, E.H., Falster, D.S., 2015. Quantifying and understanding reproductive allocation schedules in plants. Ecology and Evolution 5, 5521–5538. https://doi.org/10.1002/ece3.1802

Zeide, B., 2003. The U-approach to forest modeling. Canadian Journal of Forest Research 33, 480–489. https://doi.org/10.1139/x02-175

Zeide, B., 1993. Analysis of growth equations. Forest Science 39, 594–616. https://doi.org/10.1111/j.1461-0248.2006.00883.x

Appendices

A. Solving the ODE growth model to predict future diameter

Consider a generic model of instantaneous diameter growth rate of the form

$$\frac{dD}{dt} = z(D, \theta)\,, \qquad \text{(A. 1)}$$

where $z(D, \theta)$ can take any conceivable mathematical form and is a function of both current diameter D and some parameters θ. Given an initial diameter $D(t_0)$, knowledge of how much time has elapsed (i.e., $t_1 - t_0$), and the values of the parameters θ, we can mathematically determine the predicted future diameter $D(t_1)$ by integrating the dynamical Equation (A.1) as

$$\int_{D(t_0)}^{D(t_1)} \frac{1}{z(D, \theta)}\, dx = \int_{t_0}^{t_1} d\, t \qquad \text{(A. 2)}$$

and solving the resulting expression for the single unknown, $D(t_1)$. This is referred to as solving the model's "initial-value problem". Note that our GLMM formula (Equation 2) replaces $D(t_1)$ with μ to turn the integral from a *mathematical* expression to a *statistical* problem.

The solution to the integral on the right-hand side of Equation (A.2) is equal to the amount of time elapsed, $t_1 - t_0$. In contrast, the integral on the left-hand side of this equation depends on the mathematical complexity of the growth-rate model $z(D, \theta)$, and in some cases may not always be analytically tractable. When using the nonlinear form given by Equation 1, an analytical solution does indeed exist, and if we substitute this solution into Equation A.2 we obtain

$$\begin{aligned} &D(t_1)^{-b}\big(-cD(t_1)\big)^{b}\Gamma\big(1-b, -cD(t_1)\big) \\ &= ace^{c}(t_1 - t_0) + D(t_0)^{-b}\big(-cD(t_0)\big)^{b}\Gamma\big(1-b, -cD(t_0)\big)\,, \end{aligned} \qquad \text{(A. 3)}$$

where $\Gamma(u, v) = \int_v^{\infty} x^{u-1}\, e^{-x} dx$ is the upper incomplete gamma function. Unfortunately, this is a transcendental equation for $D(t_1)$ in that there is no way to rearrange it and obtain a single closed-form solution for $D(t_1)$. This implies that numerical methods will need to be used to find the value of $D(t_1)$ for which the left-hand side and right-hand side of Equation are equal.

B. Pairwise comparison of all growth parameters

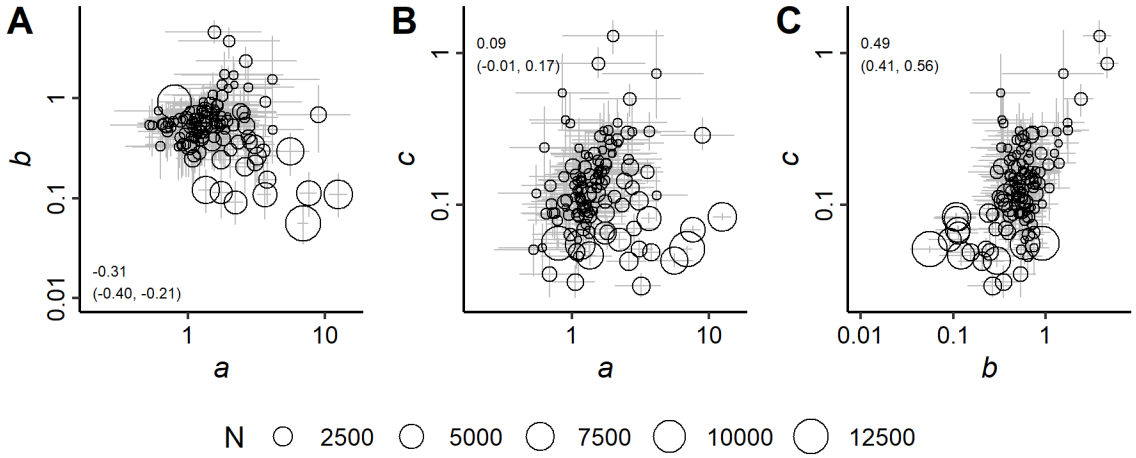

Figure S1: Pairwise comparisons of the three species-specific growth parameters: a_j (growth rate at 1-cm diameter); b_j (growth expansion factor); and c_j (growth decline factor). Points and error bars are median and 89% credible intervals (CI), respectively, of the posterior. Numbers at the corner of each panel denote the median and 89% CI of Spearman's rank correlation. Point size indicates sample size (number of trees). Note the log-scale on both axes. Panel **C** is identical to Fig. 2.

C. Species growth parameters

Table S1: Posterior median (and 89% credible intervals in parentheses) of species-specific growth parameters (see Equations 1 and 2).

Species	*a*	*b*	*c*
Acacia auriculiformis	1.97 (0.85, 4.21)	1.25 (0.61, 2.09)	0.22 (0.14, 0.34)
Adenanthera pavonina	1.84 (0.79, 4.23)	1.74 (0.83, 2.92)	0.31 (0.19, 0.49)
Adinobotrys atropurpureus	2.84 (1.65, 4.24)	0.37 (0.19, 0.64)	0.07 (0.06, 0.09)
Aleurites moluccanus	0.95 (0.54, 1.53)	0.44 (0.22, 0.78)	0.09 (0.06, 0.13)
Allophylus cobbe	2.75 (1.25, 5.98)	1.30 (0.52, 2.41)	0.30 (0.17, 0.51)
Alstonia angustifolia	1.26 (0.63, 2.32)	0.76 (0.42, 1.16)	0.09 (0.07, 0.13)
Alstonia angustiloba	0.96 (0.51, 1.73)	0.64 (0.37, 0.96)	0.06 (0.05, 0.08)
Alstonia scholaris	0.68 (0.41, 1.07)	0.54 (0.34, 0.78)	0.03 (0.02, 0.05)
Andira inermis	1.77 (0.80, 4.02)	1.38 (0.79, 2.15)	0.19 (0.13, 0.28)
Araucaria columnaris	1.08 (0.54, 2.03)	0.53 (0.26, 0.91)	0.09 (0.06, 0.13)
Arfeuillea arborescens	1.75 (1.50, 2.01)	0.11 (0.06, 0.19)	0.06 (0.06, 0.07)
Artocarpus heterophyllus	1.56 (0.77, 3.12)	0.58 (0.27, 1.11)	0.17 (0.11, 0.26)
Azadirachta indica	1.58 (0.74, 3.25)	0.68 (0.30, 1.28)	0.17 (0.10, 0.28)
Barringtonia asiatica	1.16 (0.60, 2.01)	0.57 (0.28, 0.97)	0.11 (0.07, 0.16)
Barringtonia racemosa	1.54 (0.77, 2.97)	0.65 (0.31, 1.16)	0.16 (0.10, 0.24)
Bauhinia x *blakeana*	2.14 (0.89, 4.97)	1.71 (0.89, 2.62)	0.35 (0.23, 0.49)
Brachychiton acerifolius	2.64 (1.14, 6.23)	2.38 (1.53, 3.27)	0.50 (0.38, 0.63)
Bucida buceras	1.12 (0.57, 2.06)	0.63 (0.33, 1.00)	0.08 (0.06, 0.12)
Bucida molinetii	4.14 (2.33, 7.04)	0.49 (0.22, 0.98)	0.12 (0.08, 0.18)
Callistemon viminalis	0.52 (0.27, 0.94)	0.54 (0.31, 0.84)	0.05 (0.03, 0.07)
Calophyllum inophyllum	9.01 (4.44, 15.38)	0.69 (0.28, 1.34)	0.29 (0.23, 0.38)
Calophyllum soulattri	0.69 (0.43, 1.02)	0.52 (0.25, 0.93)	0.13 (0.09, 0.20)
Cananga odorata	1.99 (0.85, 4.73)	3.77 (2.49, 5.13)	1.30 (0.99, 1.65)
Carallia brachiata	2.56 (1.27, 4.47)	0.72 (0.30, 1.35)	0.30 (0.23, 0.40)
Cassia fistula	1.74 (1.23, 2.31)	0.24 (0.13, 0.42)	0.09 (0.07, 0.10)

Species	***a***	***b***	***c***
Cassia grandis	1.15 (0.56, 2.21)	0.48 (0.23, 0.93)	0.15 (0.10, 0.21)
Casuarina equisetifolia	1.34 (0.63, 2.86)	0.75 (0.43, 1.13)	0.07 (0.05, 0.10)
Cerbera odollam	1.27 (0.64, 2.47)	0.71 (0.40, 1.09)	0.07 (0.05, 0.10)
Chrysophyllum cainito	1.64 (0.78, 3.29)	0.87 (0.42, 1.47)	0.16 (0.11, 0.25)
Chukrasia tabularis	1.34 (0.75, 2.22)	0.51 (0.27, 0.88)	0.09 (0.06, 0.13)
Cinnamomum cassia	1.06 (0.62, 1.77)	0.41 (0.19, 0.80)	0.16 (0.10, 0.24)
Cinnamomum iners	2.42 (1.18, 4.43)	0.74 (0.38, 1.20)	0.14 (0.11, 0.19)
Citharexylum spinosum	1.92 (1.02, 3.40)	0.60 (0.26, 1.14)	0.25 (0.19, 0.34)
Clitoria fairchildiana	1.10 (0.52, 2.29)	0.59 (0.31, 0.93)	0.06 (0.04, 0.09)
Coccoloba uvifera	1.11 (0.57, 2.01)	0.54 (0.27, 0.96)	0.12 (0.08, 0.19)
Cordia scabra	1.72 (0.88, 3.31)	0.52 (0.22, 1.13)	0.31 (0.20, 0.47)
Cordia subcordata	1.61 (0.87, 2.78)	0.57 (0.24, 1.18)	0.29 (0.19, 0.41)
Couroupita guianensis	1.52 (0.66, 3.44)	1.09 (0.56, 1.83)	0.13 (0.08, 0.21)
Cratoxylum cochinchinense	1.24 (0.69, 2.03)	0.46 (0.22, 0.87)	0.18 (0.13, 0.25)
Cratoxylum formosum	2.67 (1.43, 4.46)	0.53 (0.25, 0.92)	0.18 (0.15, 0.21)
Cynometra browneoides	0.88 (0.50, 1.43)	0.60 (0.31, 0.99)	0.10 (0.08, 0.14)
Cynometra cauliflora	1.30 (0.61, 2.59)	0.71 (0.38, 1.12)	0.10 (0.06, 0.15)
Cynometra malaccensis	1.13 (0.60, 2.27)	0.39 (0.18, 0.79)	0.24 (0.14, 0.37)
Cynometra ramiflora	1.05 (0.56, 1.86)	0.56 (0.27, 0.97)	0.11 (0.07, 0.17)
Cyrtophyllum fragrans	1.08 (0.81, 1.36)	0.25 (0.13, 0.41)	0.05 (0.04, 0.06)
Dalbergia latifolia	1.33 (0.68, 2.44)	0.77 (0.42, 1.17)	0.12 (0.09, 0.15)
Dalbergia oliveri	1.35 (0.68, 2.49)	0.65 (0.36, 1.02)	0.08 (0.07, 0.11)
Delonix regia	1.22 (0.59, 2.38)	0.66 (0.34, 1.09)	0.10 (0.06, 0.15)
Diospyros discolor	1.94 (0.97, 3.75)	0.67 (0.29, 1.31)	0.22 (0.14, 0.34)
Dolichandrone spathacea	0.61 (0.29, 1.28)	0.75 (0.45, 1.09)	0.05 (0.03, 0.08)
Dyera costulata	1.17 (0.66, 1.88)	0.47 (0.22, 0.85)	0.11 (0.07, 0.16)
Elaeocarpus mastersii	4.17 (1.66, 9.18)	1.55 (0.34, 4.23)	0.73 (0.37, 1.43)
Erythrophleum suaveolens	3.81 (3.06, 4.54)	0.15 (0.09, 0.26)	0.05 (0.04, 0.06)

Species	***a***	***b***	***c***
Ficus lyrata	2.59 (1.34, 4.59)	0.65 (0.30, 1.17)	0.20 (0.14, 0.28)
Filicium decipiens	2.33 (1.54, 3.29)	0.37 (0.18, 0.65)	0.10 (0.08, 0.13)
Flacourtia inermis	1.55 (1.00, 2.26)	0.41 (0.19, 0.79)	0.20 (0.14, 0.27)
Garcinia atroviridis	1.33 (0.74, 2.29)	0.44 (0.20, 0.85)	0.21 (0.14, 0.31)
Garcinia mangostana	1.34 (0.72, 2.27)	0.60 (0.28, 1.07)	0.16 (0.12, 0.22)
Garcinia subelliptica	0.55 (0.29, 0.93)	0.54 (0.26, 0.99)	0.12 (0.07, 0.18)
Gliricidia sepium	0.85 (0.39, 1.88)	0.33 (0.15, 0.68)	0.55 (0.31, 1.00)
Gnetum gnemon	2.04 (1.45, 2.75)	0.31 (0.16, 0.54)	0.11 (0.08, 0.15)
Gymnostoma nobile	0.63 (0.35, 1.30)	0.33 (0.16, 0.64)	0.24 (0.12, 0.45)
Gymnostoma rumphianum	1.53 (0.74, 3.18)	0.72 (0.31, 1.40)	0.16 (0.09, 0.29)
Hibiscus tiliaceus	1.38 (0.67, 2.62)	0.73 (0.38, 1.18)	0.13 (0.09, 0.19)
Hopea odorata	3.66 (3.22, 4.05)	0.11 (0.06, 0.18)	0.08 (0.08, 0.09)
Ilex cymosa	1.09 (0.57, 1.91)	0.60 (0.28, 1.07)	0.15 (0.10, 0.21)
Khaya grandifoliola	2.61 (1.78, 3.50)	0.21 (0.11, 0.35)	0.04 (0.04, 0.05)
Khaya nyasica	1.11 (0.59, 1.96)	0.64 (0.39, 0.93)	0.05 (0.03, 0.06)
Khaya senegalensis	5.60 (3.76, 7.75)	0.30 (0.17, 0.45)	0.04 (0.04, 0.05)
Kopsia arborea	3.58 (2.54, 4.69)	0.30 (0.14, 0.54)	0.16 (0.14, 0.20)
Lagerstroemia floribunda	1.46 (0.69, 2.85)	0.89 (0.43, 1.47)	0.22 (0.16, 0.30)
Lagerstroemia langkawiensis	3.68 (1.67, 6.83)	0.92 (0.41, 1.62)	0.31 (0.23, 0.41)
Lagerstroemia speciosa	1.30 (0.72, 2.15)	0.52 (0.25, 0.88)	0.12 (0.09, 0.15)
Libidibia ferrea	0.74 (0.42, 1.24)	0.52 (0.26, 0.86)	0.09 (0.06, 0.13)
Lophanthera lactescens	1.86 (1.00, 3.36)	0.49 (0.21, 1.01)	0.27 (0.18, 0.40)
Magnolia champaca	0.87 (0.49, 1.52)	0.41 (0.20, 0.78)	0.15 (0.10, 0.23)
Magnolia x alba	1.10 (0.64, 1.78)	0.41 (0.20, 0.75)	0.12 (0.08, 0.19)
Mangifera indica	3.09 (2.21, 3.95)	0.23 (0.12, 0.39)	0.05 (0.04, 0.06)
Maranthes corymbosa	0.90 (0.47, 1.67)	0.62 (0.32, 1.02)	0.10 (0.06, 0.15)
Melaleuca bracteata	1.50 (0.87, 2.31)	0.52 (0.25, 0.94)	0.15 (0.11, 0.21)
Melaleuca cajuputi	1.27 (0.82, 1.81)	0.41 (0.21, 0.69)	0.08 (0.06, 0.11)

Species	***a***	***b***	***c***
Melaleuca citrina	1.75 (0.94, 3.08)	0.58 (0.29, 0.95)	0.10 (0.08, 0.14)
Mesua ferrea	1.19 (0.71, 1.80)	0.49 (0.24, 0.84)	0.13 (0.10, 0.17)
Mimusops elengi	2.21 (1.93, 2.52)	0.09 (0.05, 0.15)	0.06 (0.05, 0.07)
Nephelium lappaceum	1.76 (0.91, 3.32)	0.56 (0.25, 1.13)	0.17 (0.10, 0.29)
Peltophorum pterocarpum	6.95 (6.34, 7.55)	0.06 (0.03, 0.09)	0.05 (0.05, 0.05)
Pentaspadon motleyi	1.14 (0.68, 1.85)	0.52 (0.25, 0.88)	0.11 (0.07, 0.17)
Planchonella obovata	1.51 (1.11, 1.92)	0.37 (0.20, 0.62)	0.12 (0.10, 0.15)
Plumeria obtusa	2.15 (1.18, 3.69)	0.54 (0.24, 1.09)	0.27 (0.20, 0.37)
Plumeria rubra	0.71 (0.43, 1.05)	0.46 (0.23, 0.81)	0.10 (0.07, 0.14)
Podocarpus rumphii	1.18 (0.61, 2.24)	0.45 (0.21, 0.85)	0.14 (0.08, 0.24)
Pongamia pinnata	1.21 (0.84, 1.68)	0.29 (0.15, 0.49)	0.07 (0.05, 0.09)
Pterocarpus indicus	3.20 (2.07, 4.49)	0.26 (0.14, 0.44)	0.03 (0.02, 0.04)
Samanea saman	0.79 (0.61, 1.04)	0.92 (0.80, 1.04)	0.06 (0.05, 0.06)
Sandoricum koetjape	1.81 (1.25, 2.49)	0.39 (0.21, 0.62)	0.07 (0.05, 0.08)
Saraca indica	1.17 (0.70, 1.90)	0.44 (0.21, 0.83)	0.15 (0.10, 0.23)
Saraca thaipingensis	0.73 (0.43, 1.12)	0.56 (0.30, 0.92)	0.09 (0.06, 0.12)
Schizolobium parahyba	1.57 (0.74, 3.24)	0.79 (0.38, 1.38)	0.17 (0.11, 0.26)
Sindora wallichii	0.78 (0.48, 1.22)	0.59 (0.33, 0.93)	0.08 (0.05, 0.12)
Sterculia cordata	0.90 (0.48, 1.72)	0.34 (0.16, 0.69)	0.36 (0.21, 0.57)
Sterculia foetida	1.55 (0.68, 3.45)	4.61 (3.52, 6.05)	0.86 (0.68, 1.10)
Sterculia lanceolata	1.59 (0.82, 3.10)	0.54 (0.24, 1.07)	0.19 (0.11, 0.30)
Sterculia monosperma	1.77 (0.77, 3.80)	1.07 (0.58, 1.60)	0.19 (0.14, 0.24)
Sterculia parviflora	2.75 (1.76, 4.00)	0.42 (0.21, 0.73)	0.13 (0.10, 0.16)
Suregada multiflora	0.65 (0.43, 0.92)	0.55 (0.30, 0.87)	0.09 (0.05, 0.13)
Swietenia macrophylla	1.15 (0.84, 1.60)	0.60 (0.46, 0.74)	0.05 (0.05, 0.06)
Syzygium aromaticum	1.25 (0.70, 2.18)	0.49 (0.22, 0.97)	0.21 (0.14, 0.31)
Syzygium cerasiforme	1.24 (0.81, 1.74)	0.40 (0.21, 0.69)	0.09 (0.07, 0.12)
Syzygium cumini	1.68 (0.83, 3.17)	0.54 (0.24, 1.13)	0.23 (0.14, 0.36)

Species	***a***	***b***	***c***
Syzygium glaucum	1.10 (0.87, 1.32)	0.27 (0.14, 0.46)	0.09 (0.07, 0.11)
Syzygium grande	12.64 (10.76, 14.58)	0.11 (0.06, 0.18)	0.08 (0.08, 0.09)
Syzygium incarnatum	1.60 (0.75, 3.24)	0.75 (0.37, 1.34)	0.15 (0.09, 0.24)
Syzygium myrtifolium	1.01 (0.71, 1.36)	0.33 (0.16, 0.62)	0.18 (0.14, 0.23)
Syzygium papillosum	1.03 (0.55, 1.90)	0.76 (0.39, 1.26)	0.14 (0.08, 0.22)
Syzygium polyanthum	3.11 (1.95, 4.31)	0.35 (0.18, 0.62)	0.11 (0.09, 0.13)
Syzygium zeylanicum	0.92 (0.56, 1.42)	0.34 (0.17, 0.61)	0.11 (0.07, 0.16)
Tabebuia pallida	1.44 (0.72, 2.62)	0.62 (0.31, 1.03)	0.09 (0.06, 0.13)
Tabebuia rosea	7.67 (6.52, 8.77)	0.11 (0.07, 0.18)	0.07 (0.06, 0.07)
Tamarindus indica	1.63 (0.76, 3.44)	0.84 (0.45, 1.33)	0.14 (0.10, 0.19)
Terminalia calamansanai	1.30 (0.59, 2.79)	0.92 (0.55, 1.36)	0.10 (0.07, 0.15)
Terminalia catappa	1.06 (0.72, 1.47)	0.35 (0.20, 0.53)	0.03 (0.02, 0.04)
Terminalia mantaly	1.74 (0.85, 3.28)	0.66 (0.32, 1.16)	0.14 (0.10, 0.22)
Tristaniopsis whiteana	0.97 (0.50, 1.93)	0.35 (0.16, 0.72)	0.35 (0.20, 0.56)
Vitex pinnata	2.17 (0.99, 4.74)	1.36 (0.67, 2.28)	0.25 (0.15, 0.41)
Xanthostemon chrysanthus	1.35 (1.19, 1.48)	0.12 (0.07, 0.19)	0.05 (0.04, 0.05)

714

D. Model performance

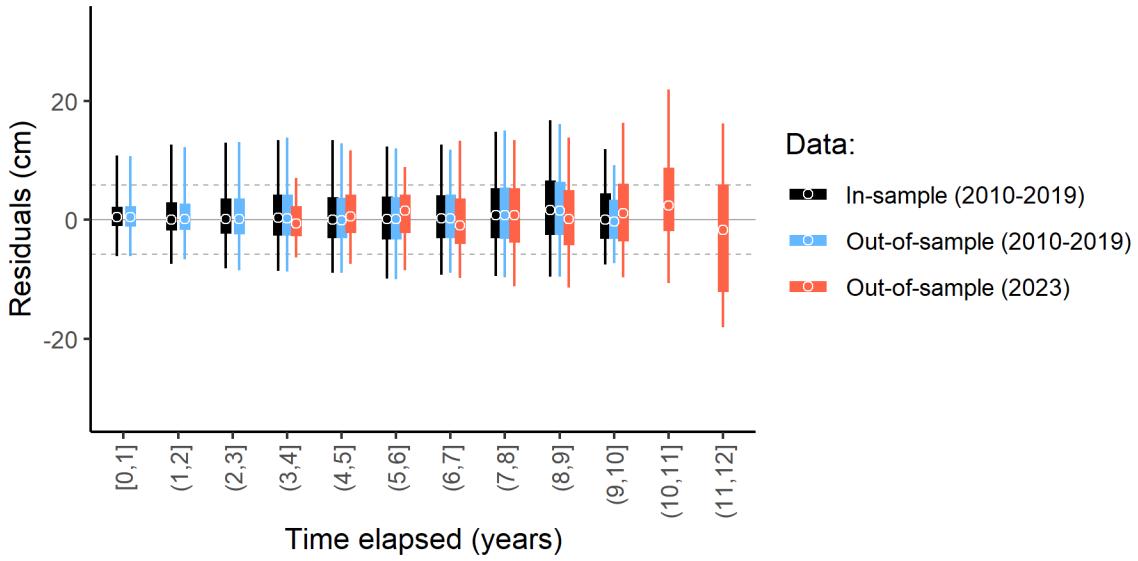

Figure S2: The relationship between residuals in diameter (i.e., observed − predicted diameter) and time lapsed between diameter measurements from in-sample (black) and out-of-sample (blue = same period 2010–2019; red = 2023) datasets. Circles are median while thick and thin bars are 50%- and 89%-tiles, respectively. For benchmarking, the horizontal lines and Y-axis limits mark the 50%- and 89-tiles of predictions, respectively, from the published models in McPherson et al., 2016. See codes accompanying this study for the calculation of the benchmark CIs.

E. Temporal transferability

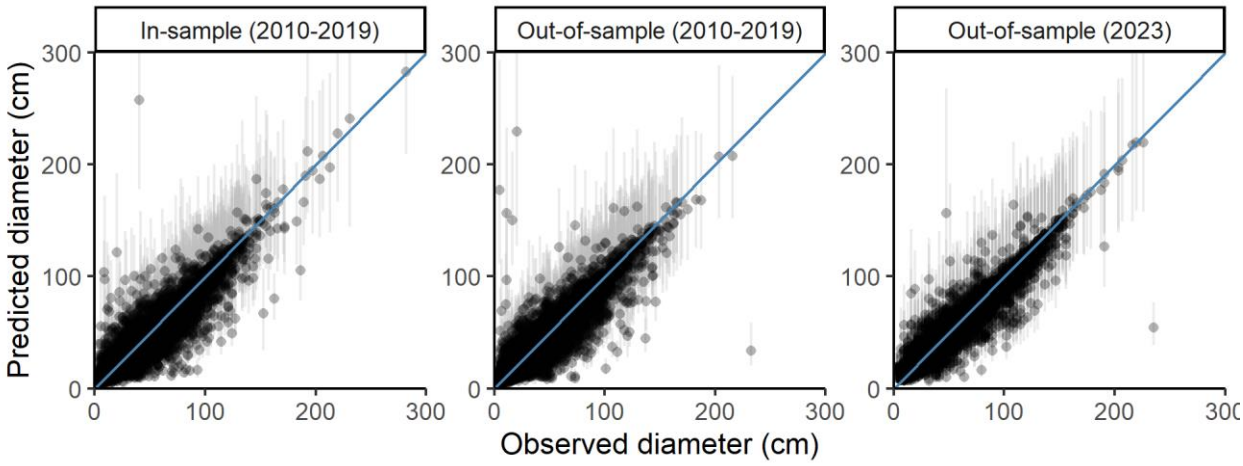

Figure S3: Validating the predicted diameter (using the model trained on 2010–2019 data) on the observed diameter of a subset of trees in the same period (left), in 2023 (middle) and an independent dataset from the United States (McPherson et al., 2016; right). Points and error bars are median and 89% credible intervals (CI), respectively, of the posterior. Blue slope denotes the 1:1 line.